

# Influence of temperature and precipitation variability on near-term snow trends

Justin S. Mankin · Noah S. Diffenbaugh

Received: 6 May 2014 / Accepted: 28 September 2014  
© Springer-Verlag Berlin Heidelberg 2014

**Abstract** Snow is a vital resource for a host of natural and human systems. Global warming is projected to drive widespread decreases in snow accumulation by the end of the century, potentially affecting water, food, and energy supplies, seasonal heat extremes, and wildfire risk. However, over the next few decades, when the planning and implementation of current adaptation responses are most relevant, the snow response is more uncertain, largely because of uncertainty in regional and local precipitation trends. We use a large (40-member) single-model ensemble climate model experiment to examine the influence of precipitation variability on the direction and magnitude of near-term Northern Hemisphere snow trends. We find that near-term uncertainty in the sign of regional precipitation change does not cascade into uncertainty in the sign of regional snow accumulation change. Rather, temperature increases drive statistically robust consistency in the sign of future near-term snow accumulation trends, with all regions exhibiting reductions in the fraction of precipitation falling

as snow, along with mean decreases in late-season snow accumulation. However, internal variability does create uncertainty in the magnitude of hemispheric and regional snow changes, including uncertainty as large as 33 % of the baseline mean. In addition, within the 40-member ensemble, many mid-latitude grid points exhibit at least one realization with a statistically significant positive trend in net snow accumulation, and at least one realization with a statistically significant negative trend. These results suggest that the direction of near-term snow accumulation change is robust at the regional scale, but that internal variability can influence the magnitude and direction of snow accumulation changes at the local scale, even in areas that exhibit a high signal-to-noise ratio.

**Keywords** Snow · CCSM3 · Climate variability · Water availability · Global warming

## 1 Introduction

Winter snow accumulation provides a vital natural resource (Barnett et al. 2005; Vivioli et al. 2007; Mote 2006) with direct consequences for ecosystems (Rood et al. 2008; Tague and Peng 2013), food (Hatfield et al. 2011; Ashfaq et al. 2013), water (Barnett et al. 2008; Taylor 2013; Hayhoe et al. 2004) and energy (Siegfried et al. 2011). Snow accumulation and cover can also have important indirect impacts via atmospheric circulation (Fletcher et al. 2009; Alexander et al. 2010; Cohen et al. 2012; Sobolowski et al. 2010), soil moisture (Sheffield et al. 2004), and surface radiative balance (Qu and Hall 2007; Bony et al. 2006; Lawrence and Slater 2009), thereby contributing to spring and summer heat extremes (Diffenbaugh et al. 2005; Hall et al. 2008) and wildfires (Westerling et al. 2006).

J. S. Mankin (✉)  
Emmett Interdisciplinary Program in Environment  
and Resources, Stanford University, 473 Via Ortega, Jerry  
Yang and Akiko Yamazaki Environment and Energy Building,  
Stanford, CA 94305-4216, USA  
e-mail: jsmankin@stanford.edu

N. S. Diffenbaugh  
Department of Environmental Earth System Science, Stanford  
University, 473 Via Ortega, Jerry Yang and Akiko Yamazaki  
Environment and Energy Building, Stanford, CA 94305-4216,  
USA  
e-mail: diffenbaugh@stanford.edu

N. S. Diffenbaugh  
Woods Institute for the Environment, Stanford University,  
473 Via Ortega, Jerry Yang and Akiko Yamazaki Environment  
and Energy Building, Stanford, CA 94305-4216, USA

Global warming is projected to cause widespread decreases in mid-latitude boreal cold-season snow accumulation and snowfall by the end of the century (Diffenbaugh et al. 2012; Ashfaq et al. 2013; Räisänen 2007; Krasting et al. 2013; Pierce and Cayan 2013), potentially impacting snow-dependent systems (Barnett et al. 2005; Diffenbaugh and Field 2013). However, two essential and covarying influences on snow—precipitation and temperature—are subject to unforced climate system variability (Hawkins and Sutton 2010; Deser et al. 2012a; Meehl et al. 2009). Such internal variability creates substantial uncertainty in the sign and magnitude of decadal-scale trends in regional and local temperature and precipitation, particularly in the near-term decades (Deser et al. 2012a, b; Hawkins and Sutton 2009, 2010). Internal variability could therefore also influence trends in snow accumulation that occur within the context of long-term global warming (Diffenbaugh et al. 2012; Howat and Tulaczyk 2005; Scherrer and Appenzeller 2006; Stewart 2009; Räisänen 2007; Hamlet et al. 2005; Mudryk et al. 2013). The confounding effects of internal variability pose particular complications for climate risk management (Kunreuther et al. 2013) over the near-term decades, when current adaptation decisions are most relevant (Carter et al. 2007; Füssel 2007) but when the change in the mean is likely to be relatively small (Diffenbaugh et al. 2012; Krasting et al. 2013; Pierce and Cayan 2013).

The transient response of snow accumulation to increasing greenhouse forcing has been explored in the multi-GCM context (Diffenbaugh et al. 2012; Ashfaq et al. 2013; Krassing et al. 2013; Räisänen 2007; Pierce and Cayan 2013). The CMIP5 ensemble shows robust declines in cold-season snow accumulation and snowfall in most Northern Hemisphere (NH) regions by the end of the twenty-first century in the IPCC AR5 RCP8.5 and RCP4.5 forcing pathways, with Northeastern Eurasia showing robust increases (Diffenbaugh et al. 2012; Krassing et al. 2013). However, over the near-term decades, a number of snow-dependent regions exhibit projected snow accumulation changes that are small relative to the inter-annual variability, and not all members agree on the sign of change (Diffenbaugh et al. 2012; Krassing et al. 2013), or show consistent responses among hydroclimatic variables (Pierce and Cayan 2013). For example, while surface air temperature signals emerge quickly in the CMIP5 RCP4.5 pathway, regional-scale snowfall signals take much longer, or never emerge at all, suggesting that snowfall may not exhibit robust regional-scale changes in response to intermediate increases in radiative forcing (Krassing et al. 2013). However, because the near-term decades are the timeframe over which regional climate adaptations are best positioned to offset future climate damages (Carter et al. 2007), quantification of irreducible uncertainty in near-term snow accumulation change is critical for adaptive response.

Despite the studies that have examined snow in the CMIP5, it is unclear whether the ensemble's uncertainty in signal emergence, particularly in the near-term, is due to internal variability, structural differences among the models, or a combination of the two (Ashfaq et al. 2013; Rupp et al. 2013; Diffenbaugh et al. 2012). Distinguishing the role of internal variability—and the associated irreducible uncertainty—requires a large number of integrations of the same model in a single forcing pathway (Deser et al. 2012a), which has not been available in CMIP. Therefore, it remains critical to examine whether internal variability alone is sufficient to create uncertainty in the direction of near-term regional and sub-regional snow accumulation trends.

Such an analysis requires a large single-model climate model ensemble. In this study, we examine the influence of temperature and precipitation variability on the direction and magnitude of NH snow accumulation trends using a unique 40-member ensemble of a single atmosphere–ocean general circulation model (GCM) (Deser et al. 2012a) (see “Methods”). The 40 integrations are given the same boundary conditions and atmospheric constituent concentrations, with each integration initialized using only minor differences in the atmospheric state (Deser et al. 2012a). The spread within the ensemble thus represents a calculation of the irreducible uncertainty arising from atmospheric noise in one forcing trajectory given one initial ocean state. Such an experiment provides the opportunity for critical insight into the range of outcomes that the natural world could manifest in response to near-term global warming (Deser et al. 2012b).

## 2 Methods

### 2.1 Climate model configuration

CCSM3.0 is a general circulation model with coupled atmosphere, ocean, land, and sea-ice components. In this experiment, called the “twenty-first century CCSM3.0 Large Ensemble Project” the atmospheric component is run with T42 spectral truncation (~2.8° resolution in the horizontal). The model is forced with the IPCC SRES A1B greenhouse-gas emissions trajectory from the IPCC AR4, in which atmospheric CO<sub>2</sub> concentrations increase from 380 to 570 ppm over the 2000–2060 integration (see Meehl et al. 2006; Deser et al. 2012a). At the end of the twenty-first century, the likely global warming in the A1B scenario falls between RCP6.0 and RCP8.5, the two highest scenarios of CMIP5 (Rogelj et al. 2012). During the first half of the twenty-first century (over which the CCSM3 ensemble is run), A1B has rates of emissions slightly higher than the RCP8.5 until 2030, at which point the rates slow through 2050 (Peters et al. 2013). The net effect of A1B is a mean

global warming level similar to the RCP8.5 over the first 60 years of the twenty-first century ( $\sim 2^\circ\text{C}$  relative to the late-twentieth century) (Knutti and Sedláček 2012), which is the time period of the CCSM3 integrations analyzed here.

Snowfall is parameterized in CCSM3 as a fraction of total precipitation as a linear function of grid-volume temperature in the model's atmospheric component, CAM3 (Collins et al. 2004). The model's land component, CLM, determines the surface accumulation of snowfall through a combination of thermodynamic and water-balance modeling, influenced by snow age, water content, and melt, which influence and are influenced by ground temperature and albedo (Oleson et al. 2004).

The 40-member ensemble is initialized from a single CCSM3 realization of the twentieth century ("20C") historical climate. The ocean, land, and sea-ice components for all 40 members were initialized using the same fields from January 1, 2000 in the single 20C integration. However, the atmospheric initial conditions were initialized with fields from 40 different days during December 1999–January 2000 from that same 20C integration (Deser et al. 2012a). The spread among the ensemble can therefore be interpreted as CCSM3's representation of internal climate variability induced by atmospheric noise, within a single forcing pathway. This intra-model spread is distinct from the intra-model spread seen in the CMIP3 or CMIP5 projections, which results from uncertainty in the initial state of the atmosphere, ocean, and sea ice. It should be stressed that because the CCSM3 intra-model spread only captures the variability induced by the atmospheric initial conditions, the intra-model model spread would be different (and perhaps larger) if the 40 runs were initialized from differing phases of low-frequency variability in the ocean or sea-ice states, as in the single-model ensembles within CMIP. Additional large-ensemble experiments will be necessary to quantify the extent to which uncertainty in model structure, level of forcing, and initial state of the ocean and sea-ice influence the uncertainty in snow trends.

We use the 1970–1999 period of the single CCSM3 20C realization from which all members were initialized as the baseline against which all 40 twenty-first century realizations are compared. We define an individual month's 'net snow accumulation' as the monthly-mean value of the IPCC variable 'surface snow amount, (snw)' ( $\text{kg m}^{-2}$ , or "snow water equivalent"). The March value, which we analyze here, is a measure of the cold-season net accumulated snow remaining in March and represents the total accumulated snowfall less the total snowmelt (and ablation) over the cold-season (Mote et al. 2005; Kapnick and Hall 2011; Bohr and Aguado 2001). Given the potential for high-latitude and high-elevation areas to exhibit snow seasons that last beyond March, we also present net snow accumulation trends for April, May, and June. Like the March value,

these monthly values represent the total accumulated snowfall less the total snowmelt (and ablation) over the cold-season up through that month.

For other variables, we define 'cold-season average' as the mean of November–March (NDJFM). Data from December 2057 in run 39 are removed from the analysis, as all values were coded as '0' on the Earth System Grid ([www.earthsystemgrid.org](http://www.earthsystemgrid.org); the database from which the CCSM3 data were downloaded). As a result, for the year 2057 of run 39, the seasonal NDJFM average is calculated using the values from November, January, February and March. This calculation does not influence the snow accumulation results, but rather only the variables calculated at the seasonal scale (NDJFM). Although this recoding does influence the mean seasonal values calculated in the year 2057 of the single run, it avoids removing the 2057 value from the time series, which, given the placement of 2057 near the end of the 2000–2060 time series, could bias the calculation of the linear trend.

## 2.2 Model validation

Given that the focus of our analysis is the interaction among temperature, precipitation and snow accumulation, we seek to compare the 20C simulation of historical climate to a single observational dataset that provides physical consistency among the three variables. We therefore employ reanalysis output from version 2.0 of the Global Land Data Assimilation System (GLDAS-2) (Rodell and Houser 2004). The GLDAS-2 assimilates global meteorological observations and simulates observed land surface processes from 1948 to 2010. Land surface variables are available at  $0.25^\circ$  horizontal resolution.

Following Diffenbaugh et al. (2012), we compare the geographic extent of snow accumulation in the GLDAS-2 and CCSM3 by identifying the grid points with any snow accumulation in any month during the baseline period (1970–1999). In addition, we compare the relationship between March net snow accumulation and cold-season (NDJFM) temperature and precipitation for the 9 regions analyzed (as well as the Northern Hemisphere). We first calculate the area-weighted mean and interannual standard deviation in CCSM3 and GLDAS-2 for the baseline. We then calculate the difference between the respective CCSM3 and GLDAS-2 values, and divide the difference by the GLDAS-2 mean to yield the CCSM3 bias as a percent difference from GLDAS.

## 2.3 Calculation of hemispheric, regional, and grid point linear trends

We use the time series of monthly-mean values to estimate autocorrelation-corrected (generalized least squares)

**Table 1** Regional domains and number of grid points used in the analysis based on T42 spectral truncation

Region	Latitude (degrees north)	Longitude (degrees east)	No of grid points
Northern Hemisphere	20–90	0–360	3,200
(1) Alaska	51.6257–73.9475	191.25–255.938	216
(2) Arctic Canada	51.6257–73.9475	255.938–300.938	135
(3) W. US	29.3014–51.6257	230.625–255.938	63
(4) E. US	34.8825–51.6257	255.938–300.938	75
(5) N. Europe	46.0447–71.1578	0–30.9375	99
(6) N.E. Europe	46.0447–71.1578	30.9375–61.875	96
(7) N.E. Asia	46.0447–71.1578	61.875–182.812	344
(8) Central Asia	26.5108–46.0447	39.375–64.6875	80
(9) Greater Himalaya	29.3014–46.0447	64.6875–106.875	105

linear time trends in monthly and cold-season average for five variables: (1) March net snow accumulation ('snw',  $\text{kg m}^{-2}$ ), (2) cold-season near surface temperature ('tas',  $^{\circ}\text{C}$ ), (3) cold-season precipitation ('pr',  $\text{kg m}^{-2} \text{s}^{-1}$ ), (4) cold-season snowfall flux ('prsn',  $\text{kg m}^{-2} \text{s}^{-1}$ ), and (5) cold-season snowfall-to-precipitation ratio (the trends of which we present as a percentage of the baseline mean ratio). We estimate linear trends in all 40 ensemble members for these variables at the hemispheric, regional, and grid point ("sub-regional") scales. We also calculate trends for net snow accumulation, mean monthly snowfall, and the mean monthly snowfall-to-precipitation ratio for the months of March, April, May, and June to examine snow trends at higher latitudes where the snow season may be longer.

We estimate Northern Hemisphere (20 N to 90 N latitude) and regional (see Table 1) area-weighted averages over land and fit linear trends to those averages for each realization for the 2000–2060 period. We also fit individual grid point linear trends for each realization for the 2000–2060 period.

Trends in precipitation, snow accumulation, and snowfall are expressed as percentages of the seasonal (precipitation and snowfall) or monthly (snow accumulation) baseline value. We use the entire 2000–2060 integration period to calculate the trend coefficients, and then multiply the resultant coefficient by 50 years. Thus the trends can be read as 'percent change per 50 years'. At all scales, each time series is fit with an ordinary least squares (OLS) regression estimate as a function of time. Because autocorrelation can lead to an overestimate of statistical significance in linear trends (Santer et al. 2000), we test the residuals off this OLS coefficient for autocorrelation. If autocorrelation is significant (5 % level, assuming normality of the autocorrelation statistic), we fit a generalized least squares (GLS) model estimated using an autoregressive moving average process of order  $p = 1$  or  $p = 2$ , based on the data's covariance structure (estimated from the partial autocorrelation function of the data). Fitting a GLS allows us to estimate the significance of the trend correcting for

autocorrelation of the residuals. For significance of individual trends, we test the time coefficient based on the standard Student's  $t$  score given a preselected  $\alpha$ -level:  $\text{Pr}(>|t|) < \alpha$ , using  $\alpha = 0.05$  or  $\alpha = 0.01$ .

Ensemble trends are calculated as the average of the 40 single-realization trends. Ensemble trend significance (robustness) is calculated as the signal-to-noise ratio, S/N, of the ensemble average trend to the standard deviation (SD) of the 40 individual trends. For the regional-scale, ensemble trend values are calculated as the trend fitted to the ensemble average area-weighted time series to allow estimation of a  $p$  value. We compare this regional-scale ensemble trend calculated to the average of all 40 regional-scale trends, and find that they are the same for all regions. For regional-scale trends, we present two measures of statistical significance: first, as a typical significance test of a time trend, and second, as an ensemble S/N (Table 2). The counts of statistically significant individual regional-scale trends and their direction are presented in Table 3.

Note that the regions analyzed have different numbers of grid points over which the climate signal and noise are compared. While this allows for evaluation of signal emergence across variables within each region, differing region sizes can influence the S/N, making comparisons of S/N across regions difficult. We therefore only use the S/N to compare variables within regions, rather than across regions. At the grid point scale, S/N can be compared.

For the nonlinear regression, we use the visually-weighted regression method, which uses color-saturation and contrast to represent regression estimate uncertainty (Hsiang 2013). We resample the times series of area-weighted average over-land Northern Hemisphere data, estimating a new nonlinear regression estimate with each sample. We use the entire series to weight each local regression estimate (using the 'loess' function in the statistical software R, given the smoothing parameter  $\alpha = 1$ ). Each regression estimate is plotted with the same degree of transparency; as more estimates overlap, a region of higher opacity emerges representing the 95 % confidence interval

**Table 2** Ensemble 50-year trends for net snow accumulation, and seasonal temperature, precipitation, snowfall, and snowfall-to-precipitation ratio estimated from 2000 to 2060

Region	Net snow trend [% 50 years <sup>-1</sup> ] (S/N)	NDJFM temperature trend [°C 50 years <sup>-1</sup> ] (S/N)	NDJFM precipitation trend [% 50 years <sup>-1</sup> ] (S/N)	NDJFM snowfall trend [% 50 years <sup>-1</sup> ] (S/N)	NDJFM ratio trend [% 50 years <sup>-1</sup> ] (S/N)
(1) Alaska	-21.27* (3.38)	3.35* (4.40)	13.82* (4.29)	-5.49* (1.23)	-14.57* (4.60)
(2) Arctic Canada	-3.74* (1.69)	4.15* (8.05)	15.91* (5.05)	6.32* (2.29)	-6.32* (5.95)
(3) W. US	-44.93* (2.60)	1.65* (3.72)	<b>-1.70 (0.37)</b>	-20.64* (3.60)	-18.25* (3.23)
(4) E. US	-21.98* (2.27)	1.96* (4.17)	6.08* (1.49)	-11.98* (2.42)	-15.60* (3.39)
(5) N. Europe	-29.72* (1.89)	1.84* (3.88)	4.49* (1.84)	-29.02* (3.30)	-30.00* (3.62)
(6) N.E. Europe	-22.82* (4.83)	2.87* (4.12)	9.35* (3.71)	-14.32* (5.16)	-20.57* (6.49)
(7) N.E. Asia	<b>0.74 (0.40)</b>	3.57* (6.12)	16.23* (6.36)	8.64* (4.12)	-5.81* (7.22)
(8) Central Asia	<b>-11.98* (0.62)</b>	1.65* (5.73)	<b>-4.68* (0.96)</b>	-35.99* (3.55)	-36.02* (3.53)
(9) Greater Himalaya	-10.96* (1.43)	2.11* (6.09)	3.74* (1.02)	-7.10* (1.90)	-10.29* (6.97)

All trends are expressed as percentages of the baseline (1970–1999) mean, save for temperature, which is in Celsius. We show two measures of statistical significance. The first number in each row is the ensemble linear trend with an asterisk (\*) next to those trends that are statistically significant at the 1 % level. The number in parentheses indicates the signal-to-noise ratio (S/N) of that ensemble average trend relative to all trends within the ensemble—a number greater than one indicates an ensemble trend greater than  $\pm$  standard deviation of the ensemble variability. Note that comparison of the S/N across regions may be influenced by the varying sizes of the regions (see “Methods”). Bolded results are those that do not show significance in at least one of the two significance tests

**Table 3** Number of realizations (out of 40) with statistically significant linear trends (autocorrelation-corrected) and their direction (positive or negative) for five variables given area-weighted averages in the nine regions, estimated from 2000 to 2060

Region	Net snow ( $p < 0.05$ )	NDJFM temperature ( $p < 0.01$ )	NDJFM precipitation ( $p < 0.05$ )	NDJFM snowfall ( $p < 0.05$ )	NDJFM ratio ( $p < 0.05$ )
(1) Alaska	39 (-)	39 (+)	39 (+)	11 (-)	40 (-)
(2) Arctic Canada	6 (-)	40 (+)	40 (+)	22 (+)	40 (-)
(3) W. US	26 (-)	38 (+)	2 (-)	37 (-)	32 (-)
(4) E. US	19 (-)	38 (+)	10 (+)	24 (-)	36 (-)
(5) N. Europe	16 (-)	39 (+)	22 (+)	38 (-)	39 (-)
(6) N.E. Europe	39 (-)	38 (+)	35 (+)	39 (-)	40 (-)
(7) N.E. Asia	2 (+/-)	40 (+)	40 (+)	37 (+)	40 (-)
(8) Central Asia	4 (-)	40 (+)	2 (-)	36 (-)	38 (-)
(9) Greater Himalaya	19 (-)	40 (+)	11 (+)	23 (-)	40 (-)

‘Ratio’ refers to the ratio of cold-season (NDJFM) snowfall to cold-season precipitation. In Northeastern Asia, one run shows a significant positive trend, one run, a significant negative trend (+/-)

around the median regression estimate, whose location is revealed as a contrasted white line (Hsiang 2013).

#### 2.4 Calculation of regional multi-decadal changes

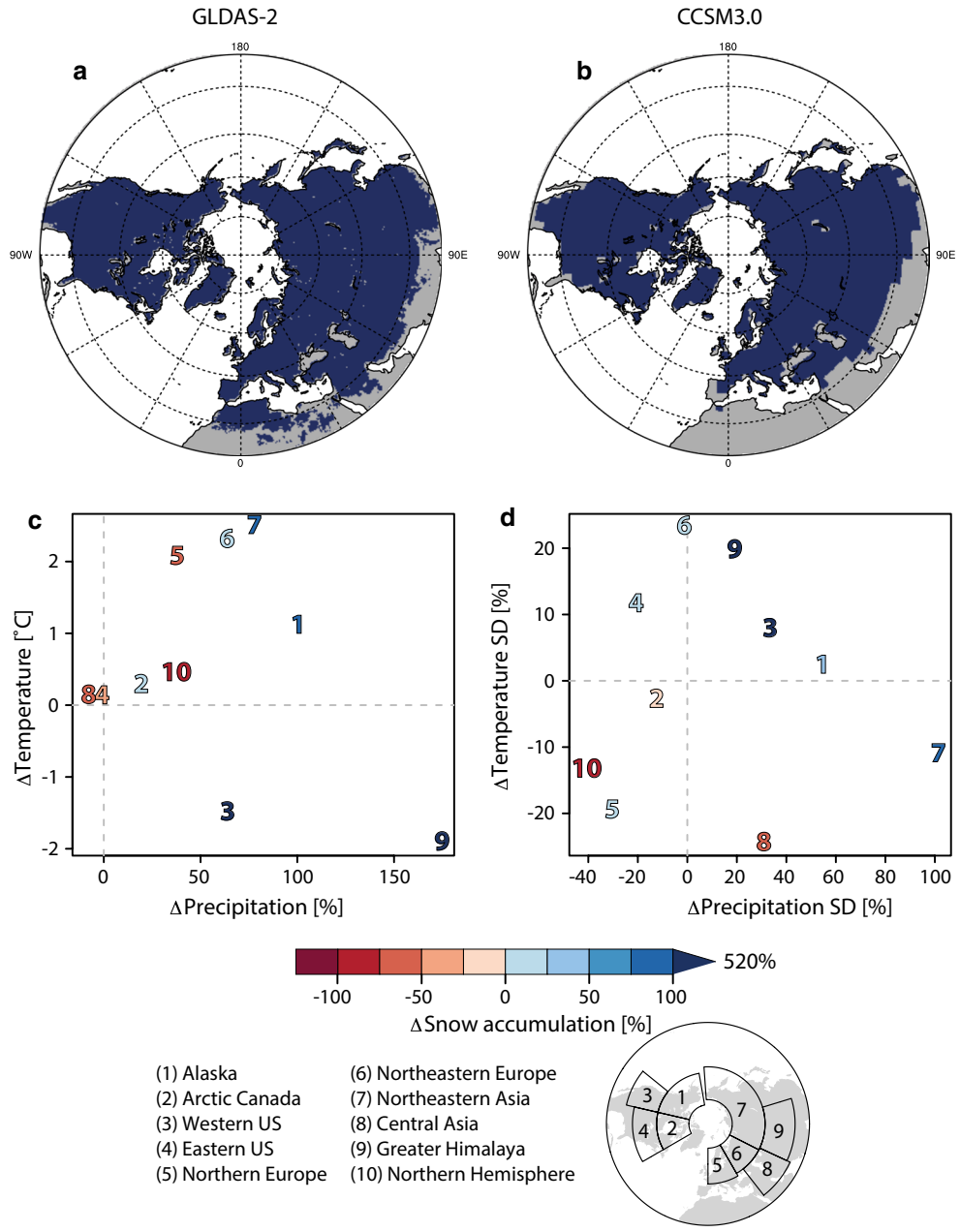
We calculate the changes in the 30-year area-weighted average snow accumulation, snowfall, precipitation, snowfall-to-precipitation ratio, and temperature for each realization over nine mid- and high-latitude regions (Table 1, defined in Diffenbaugh et al. 2012). These changes are calculated as the difference between the 2031–2060 mean in each realization and the 1970–1999 baseline in the single 20C integration. The ensemble mean and standard

deviation are both expressed as percentages of the baseline mean, save for temperature, which is presented in °C.

#### 2.5 Calculation of partial correlations

For each grid point, we estimate the Spearman’s rank non-parametric partial correlation of March net snow accumulation with cold-season precipitation and with cold-season temperature, controlling for the covarying relationship between temperature and precipitation. The Spearman’s rank makes no assumptions about the data sample’s underlying distribution. We calculate the statistical significance using the standard assumption that the Spearman’s  $\rho$

**Fig. 1** CCSM3 model validation. Areas with (dark blue) and without (grey) a monthly snow accumulation amount of at least  $0.01 \text{ kg m}^{-2}$  in any month between the period of 1970–1999 in the GLDAS-2 reanalysis (a) and the CCSM3 model (b). Grey grid points in (a) are inland bodies of water not captured by the CCSM3. The bias in the mean (c) and interannual variability ( $1\sigma$ ) (d) of seasonal temperature (y-axis), seasonal precipitation (x-axis), and March snow accumulation (color scale) in the CCSM3 for the 9 regions analyzed plus the Northern Hemisphere for 1970–1999 (see inset map and Table 1). All values (except for the y-axis in (c), which is a simple difference) are expressed as the percent difference from the GLDAS climatology. The sign of the value expresses the direction of the bias. The color scale for snow accumulation represents mean (c) and SD (d) values. Values falling on the origin represent agreement with the GLDAS reanalysis



statistic approximates the t-distribution when  $n > 10$  under the null hypothesis that the correlation is zero.

### 3 Results

#### 3.1 Model validation

We assess CCSM3's temperature, precipitation, and snow accumulation biases against GLDAS-2 (Fig. 1). Snow accumulates over a similar geographic extent in the CCSM3 and GLDAS-2 (Fig. 1a, b). There is a negative bias in both the mean (Fig. 1c, number 10) and inter-annual

variability (Fig. 1d, number 10) of NH-mean March snow accumulation. There is also considerable inter-regional spread in the magnitude and direction of biases for the nine regions within the NH. Alaska, Arctic Canada, the Western US, Northeastern Europe, Northeastern Asia and the Greater Himalaya (regions 1, 2, 3, 6, 7, and 9) exhibit positive March snow accumulation biases (Fig. 1c). Of these, Alaska, Arctic Canada, Northeastern Europe, and Northeastern Asia (regions 1, 2, 6, and 7) also have positive temperature and precipitation biases. Positive snow accumulation, temperature, and precipitation biases over these regions suggest that even with warmer-than-observed temperatures, these regions remain below freezing (Fig. 1c). In

contrast, the positive temperature bias in Northern Europe may be sufficient to drive the negative snow accumulation bias exhibited over that region (Fig. 1c). The inter-annual variability in temperature and precipitation is larger-than-observed in Alaska, the Western US, and Central Asia (regions 1, 3 and 9), leading to larger-than-observed inter-annual variability in net snow accumulation (Fig. 1d).

Regional-scale biases in CCSM3-simulated surface air temperature (John and Soden 2007) could account for some of the CCSM3 snow bias (Krasting et al. 2013). For example, the cold biases in the Western US and the Greater Himalaya (regions 3 and 9) are associated with large positive precipitation and net snow accumulation biases, suggesting greater accumulation of snowfall. A cold bias could also result in an attenuated seasonal and inter-seasonal snow albedo feedback (SAF) (Hall and Qu 2006). A weaker-than-observed SAF would reduce cold-season snowmelt, accumulating more snow, which would affect the response of regional temperature, circulation, snow accumulation, and snowmelt to global warming (Rauscher et al. 2008; Fletcher et al. 2009; Hall et al. 2008). The size of the snow accumulation bias in CCSM3 is similar in magnitude to the biases seen in CMIP3 and CMIP5 (Roesch 2006; Diffenbaugh et al. 2012). While our analyses assume that the precision of the ensemble (the spread due to internal variability) is not influenced by these model biases, this assumption requires further testing (e.g., as in Hall and Qu 2006).

### 3.2 Hemispheric-scale snow response

At the hemispheric scale, all 40 realizations exhibit positive trends in cold-season temperature, positive trends in cold-season precipitation, and negative trends in net accumulated cold-season snow (Fig. 2c). Although these results suggest that increasing temperature overcomes increasing precipitation to create net decreases in accumulated snow, there is substantial variation in the magnitude and spatial pattern of the trends within the ensemble (Fig. 2b). Because the response to increasing forcing tends to be most robust at larger spatial scales and over longer timescales (Hawkins and Sutton 2009; Cane 2010; Meehl et al. 2009), the ensemble might be expected to show climatological convergence at the hemispheric scale. This is because of the long timescale of a half-century of integration and the large geographic area over which the noise induced by the atmospheric initial conditions is being averaged. However, 50-year trends in net accumulated NH snow range between  $-2$  and  $-12 \text{ kg m}^{-2}$  (Fig. 2c), with the realizations exhibiting the maximum and minimum changes differing by up to 14 % of the baseline mean (Fig. 2a). This range is larger at the grid point scale, where trend differences between these two realizations reach up to 280 % of baseline mean in the

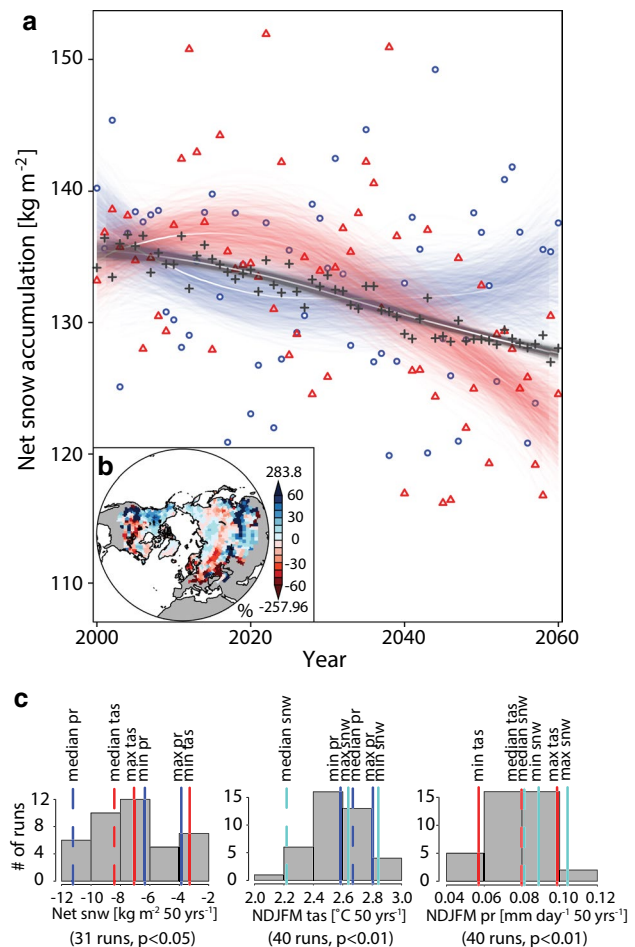


**Fig. 2** Spread in snow accumulation, temperature, and precipitation trends. **a** Simulated 2000–2060 trends in net cold-season snow accumulation (calculated as March snow water equivalent). We show the realization with the maximum (*open blue circles*) and the minimum (*open red triangles*) Northern-Hemisphere area-weighted linear trend, along with the annual mean of the 40-member ensemble (*grey plus signs*). Fitted to each of the three series is a locally weighted (non-linear) regression (see “*Methods*”). The *shading* (*blue* for the maximum trend, *red* for the minimum, and *grey* for the ensemble mean) represents the 95 % confidence interval around the median nonlinear regression estimate. **b** The map of the difference between the maximum and minimum linear 50-year snow accumulation trends among the runs plotted in **a**, where the trends are expressed as a percentage of the baseline net mean snow accumulation. *Grey* indicates regions with no snow accumulation in the baseline. **c** Histograms of the 2000–2060 area-weighted Northern Hemisphere linear trends calculated from the 40 ensemble members for net snow accumulation (snw), November–March (NDJFM) surface air temperature (tas), and NDJFM precipitation (pr). Within each histogram we mark the respective trends for the realizations that exhibit the maximum, minimum, and median snw, tas, and pr linear trends among the ensemble. We report the number of realizations showing statistically significant trends below the histograms

mid-latitudes (Fig. 2b). In addition, the realizations that show the largest hemispheric-scale declines in net snow accumulation do not exhibit the largest hemispheric-scale

**Fig. 3** Regional temperature, snow accumulation, precipitation, snowfall, and snowfall-to-precipitation ratio trends. For each of the nine regions analyzed, we show the 50-year autocorrelation-corrected linear trends of **a** NDJFM surface temperature, **b** March net snow accumulation, **c** NDJFM precipitation, **d** NDJFM snowfall, and **e** NDJFM snow-to-precipitation ratio estimated from 2000–2060. Net snow accumulation, precipitation, snowfall, and snowfall-to-precipitation ratio trends are expressed as percentages of their baseline means. The *boxplots* show the median (heavy black line) of the ensemble within a 25th to 75th percentile box, with whiskers extending to the first sample point that is less than 1.5 times the interquartile range. Realizations beyond this range are represented as *open circles*

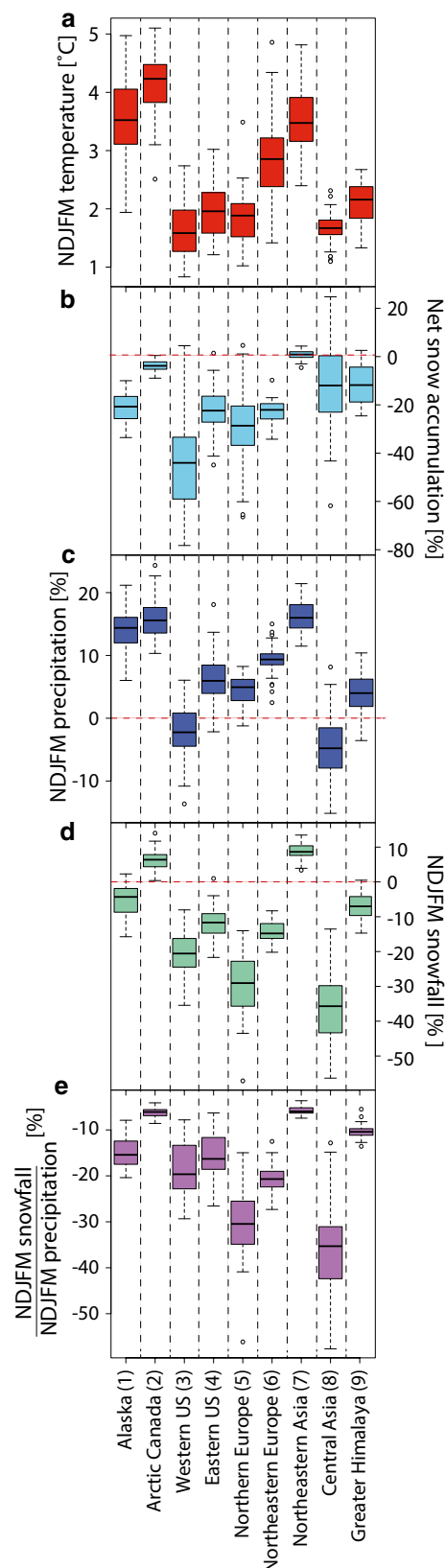
increases in temperature or decreases in precipitation (Fig. 2c). This hemispheric-scale discrepancy implies that spatial variability could play an important role in determining the variability in hemispheric-scale snow changes.

### 3.3 Regional scale snow response

Seven of the nine regions analyzed have statistically significant negative ensemble mean snow trends, with regional snow declines of 3–44 % per 50 years (Fig. 3b; Table 2). In addition, only Northeastern Asia exhibits both positive and negative snow trends that are statistically significant (Table 3). While temperature trends are consistently positive across all ensemble members and regions, the magnitude varies by a factor of 5 between the different regions. In addition, the magnitude of regional temperature trends can vary substantially across the realizations, including a range of up to 3 °C across the realizations over Arctic Canada (Fig. 3a).

In contrast to the consistency of direction in the temperature response, the intra-ensemble variation spans positive and negative precipitation trends in 5 of the 9 regions (Fig. 3). Such variability in regional-scale precipitation trends can be large relative to a region's ensemble mean trend. For example, the Western US and Central Asia (regions 3 and 8) have intra-ensemble variation equivalent to nearly 20 % of the baseline mean (Fig. 3), while their 50-year ensemble mean trends are between –1 and –5 % (Table 2).

Analysis of the multi-decadal changes (Fig. 4) illustrates the relationship between this precipitation uncertainty and regional snow changes. All realizations show declines in the fraction of precipitation falling as snowfall for all 9 regions (Fig. 4e). In addition, all realizations exhibit decreases in multi-decadal mean net snow accumulation for 7 of the 9 regions (Fig. 4a). Only Arctic Canada and Northeastern Asia (regions 2 and 7) show any realizations that exhibit increases in multi-decadal mean net snow accumulation,



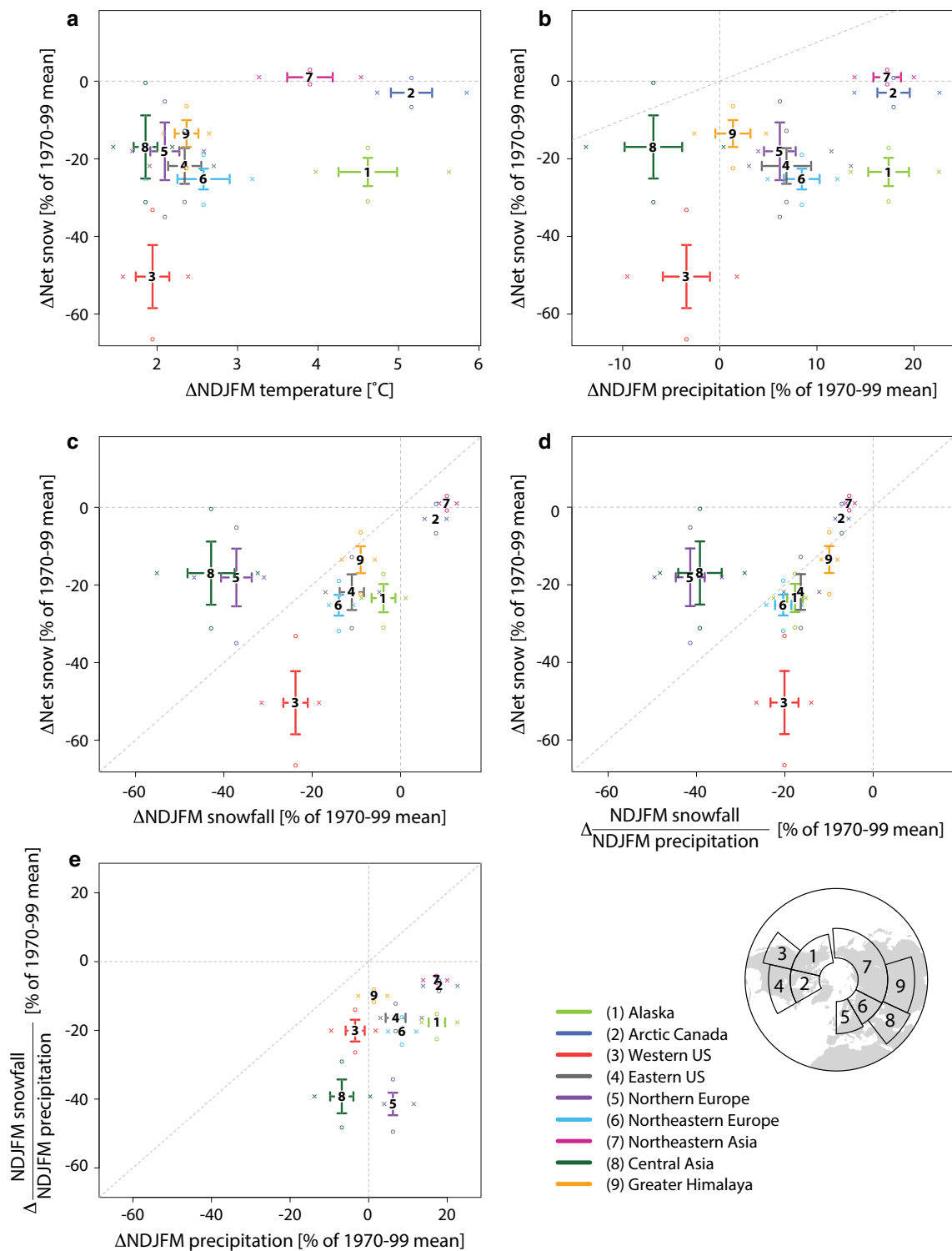
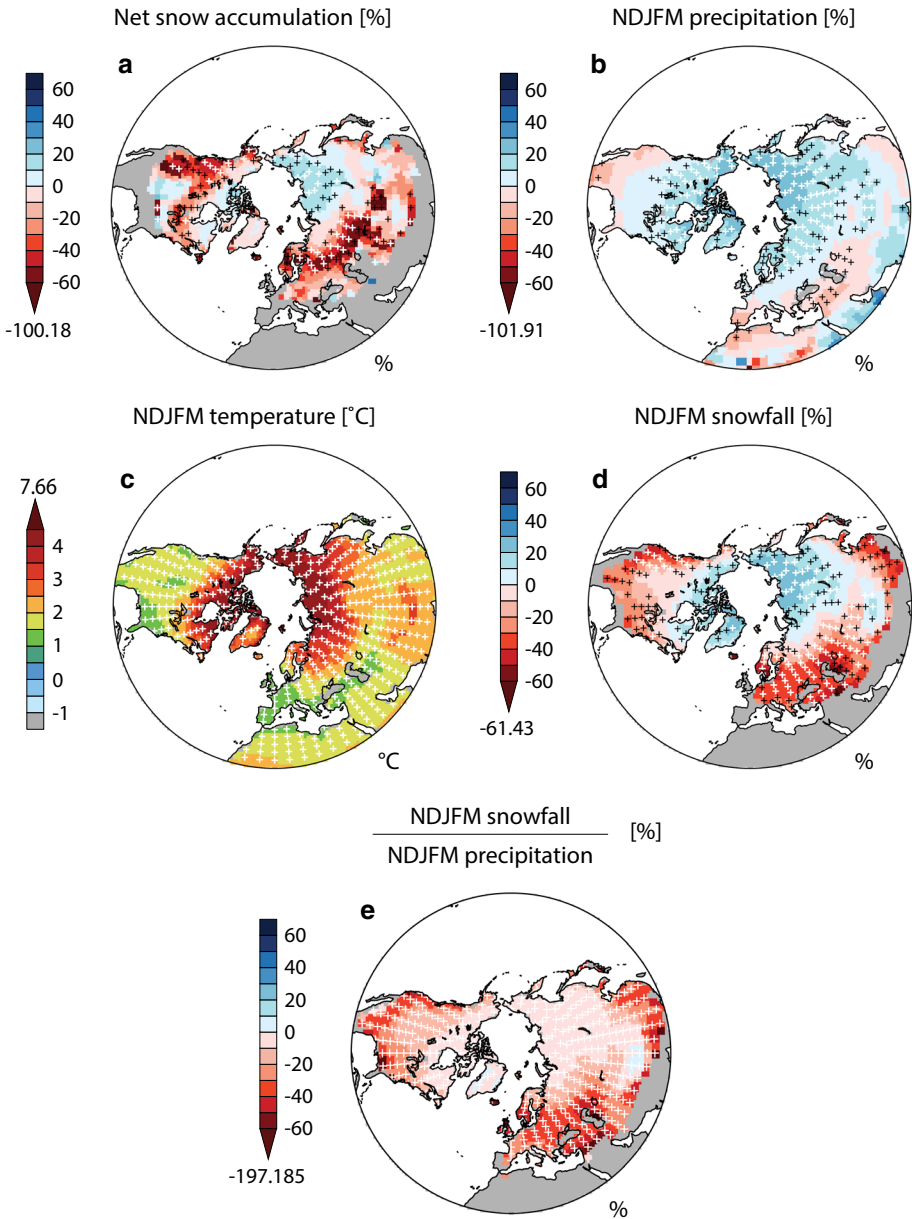


**Fig. 4** Regional changes in net snow accumulation, temperature, precipitation, and snowfall. Regional March net snow accumulation multi-decadal changes (2031–2060 minus 1970–1999) as a function of changes in cold-season (NDJFM) **a** temperature, **b** precipitation, **c** snowfall, and **d** snowfall-to-precipitation ratio for nine regions (see *inset map* and Table 1). We also show the change in snowfall-to-precipitation ratio as a function of changes in precipitation (**e**). The con-

fidence intervals around the area-weighted ensemble-mean changes represent  $\pm$  one standard deviation of the ensemble variability. Snow, precipitation, and snowfall are expressed as percentages of their baseline mean. Open circles and x's represent the most extreme ensemble member for the variable on the y and x-axes, respectively. For reference, the line of slope 1 through the origin is shown as a dotted line in **b**, **c**, **d**, and **e**

**Fig. 5** Ensemble-mean snow accumulation, temperature, precipitation, and snowfall trend maps. Color contours show the 40-member ensemble mean percent change per 50 years (linear trend) in **a** March net snow accumulation, cold-season **b** precipitation, **c** surface air temperature, **d** snowfall, and **e** snowfall-to-precipitation ratio estimated from 2000 to 2060. Snow accumulation, precipitation, and snowfall trends are expressed as percentages of their respective baseline means. Grey indicates regions with no net snow accumulation in the baseline. Stippling indicates the significance of the ensemble-mean trend, with white (black) plus signs indicating an ensemble average trend greater than two (one) times the SD of all 40 individual trends



with cold-season precipitation and snowfall increasing in all realizations over both regions (Fig. 4b, c). In contrast, all ensemble members show increases in mean cold-season precipitation but decreases in mean net snow accumulation over Alaska, the Eastern US, and Northern Europe (Fig. 4b). The ensemble spans both positive and negative changes in precipitation over the Western US, Central Asia, and the Greater Himalayas (regions 3, 8, and 9). However, all realizations exhibit declines in net snow accumulation, snowfall, and the fraction of precipitation falling as snowfall over all three of those regions (Fig. 4c, d, e). This suggests that the uncertainty in the change in regional-scale precipitation does not dictate uncertainty in the change in net snow accumulation.

### 3.4 Sub-regional-scale snow response

Many sub-regional areas show consistent trends in March net snow accumulation across the 40-member ensemble (Fig. 5a). For example, western North America, Central Canada, and Northern Europe and Eastern Europe all show robust decreases of 30–50 % per 50 years. Likewise, portions of the high-latitude Asian interior show moderate but robust March increases of ~10 % or more per 50 years.

Seasonal surface temperature trends are positive everywhere, with nearly all ensemble members, grid points, and regions exhibiting a robust signal (Fig. 5c). In general, high-latitudes and continental interiors warm more rapidly

than lower-latitude maritime regions. Precipitation shows strong agreement in the high-latitudes, with statistically significant increases of up to 20 % per 50 years (Fig. 5b). The ensemble exhibits considerably less agreement in precipitation trends over the mid-latitudes, with most mid-latitude sub-regions in North America and Europe failing to show S/N ratios greater than one.

As was seen at the regional scale, many areas exhibit greater uncertainty in precipitation trends than in temperature and snow accumulation trends (Fig. 3; Table 2). For example, in the Western US, where up to 70 % of river discharge is from snowpack (Howat and Tulaczyk 2005), the ensemble mean precipitation trend is  $-1.7\%$  over 50 years (not statistically significant), with a S/N of 0.37 (Table 2). However, net snow accumulation trends are approximately  $-40\%$  (significant at the 1 % level), and have a S/N of greater than 2. Other regions for which snow accumulation trends are more robust than precipitation trends include Northern Europe, Northeastern Europe, the Eastern US, and the Greater Himalaya (Table 2). The presence of robust declines in March net snow accumulation within the context of uncertain trends in cold-season precipitation suggests that cold-season warming drives snow trends in many areas. (It should be noted that at the regional-scale, differences in area-weighted S/N reflect not only difference in climate variability, but also the size of the regions; see “[Methods](#)”).

We test the relative influence of temperature and precipitation on the pattern of snow trends by estimating their partial correlation with March net snow accumulation in the baseline and future periods (Fig. 6). The partial correlation reveals clear patterns of precipitation and temperature influence on net snow accumulation during the baseline period (Fig. 6a, c, left column). For example, net snow accumulation variability over cold high-latitude areas tends to have a stronger relationship with precipitation variability (Fig. 6c), while its variability over warmer mid-latitude areas tends to have a stronger relationship with temperature variability (Fig. 6a). The most prominent exceptions are areas in the mid-latitude continental interiors that share a stronger correlation with precipitation (Fig. 6c), and high-latitude maritime areas that share a stronger correlation with temperature (Fig. 6a).

The partial correlation also reveals a general intensification of temperature influence on variability in net snow accumulation during the future period (Fig. 6b, d, right column). This intensification has three attributes: (1) increasing strength of the negative partial correlation with temperature in the mid-latitudes; (2) increasing strength of the positive partial correlation with temperature in the high-latitudes of Northeastern Asia; and (3) transition of many high-latitude areas from little partial correlation with temperature in the baseline period to negative partial correlation with temperature in the future period. The high ensemble agreement in the spatial pattern of future correlations

(Fig. 6e) suggests that internal variability does not influence whether a grid point is more correlated with temperature or precipitation.

The positive (but not statistically significant) correlation between high-latitude continental Asian interior temperature and snow accumulation is a notable departure from the inverse relationship between the two elsewhere (Fig. 6b). However, its correlation structure mimics the spatial pattern of ensemble mean net snow accumulation trends shown in Fig. 5a. This positive snow-temperature correlation structure over Siberia (Fig. 6b) is also associated with highly significant positive snow-precipitation correlations (Fig. 6d) and arises from at least three factors: (1) Despite large increases, regional cold-season temperatures remain cold enough to support snowfall and snow accumulation; (2) the warming advects greater Arctic moisture into the region (Deser et al. 2010); and (3) the high-latitude cold-season warming is confined to the boundary layer due to sea-ice loss, reducing the prevailing inversion, and inducing greater atmospheric instability (Deser et al. 2010). In addition, it should be noted that the high-latitude areas show decreases in net snow accumulation later in the year (Fig. 7a–d). Such late-season high-latitude decreases suggest a systematic decrease in mean net snow accumulation during the latter part of the local snow season, which generally occurs later in the year at higher latitudes and higher elevations (see “[Discussion](#)”).

## 4 Discussion

### 4.1 Influence of temperature and precipitation variability on snow trends

Decline of Northern Hemisphere snow accumulation and snow cover is seen in observations (Hartmann et al. 2013), and is a robust long-term response to increasing greenhouse forcing over most NH regions in the CMIP5 ensemble (Diffenbaugh et al. 2012). This response holds even at lower forcing levels, such as in RCP4.5 (Krasting et al. 2013). However, the influence of internal variability on the direction and magnitude of near-term snow accumulation trends is less clear, particularly at the sub-regional spatial scales that could be most useful for adaptation planning. Quantifying this near-term irreducible uncertainty in snow changes is a critical component of climate risk management (Kunreuther et al. 2013), and requires an experimental design that to-date has been unavailable in CMIP.

Although we find that the direction of the regional-scale snow response is consistent across the large single-model ensemble, the magnitude can vary by 3–33 % between individual realizations, depending on the region (Table 4). Indeed, within the 40-member ensemble, many

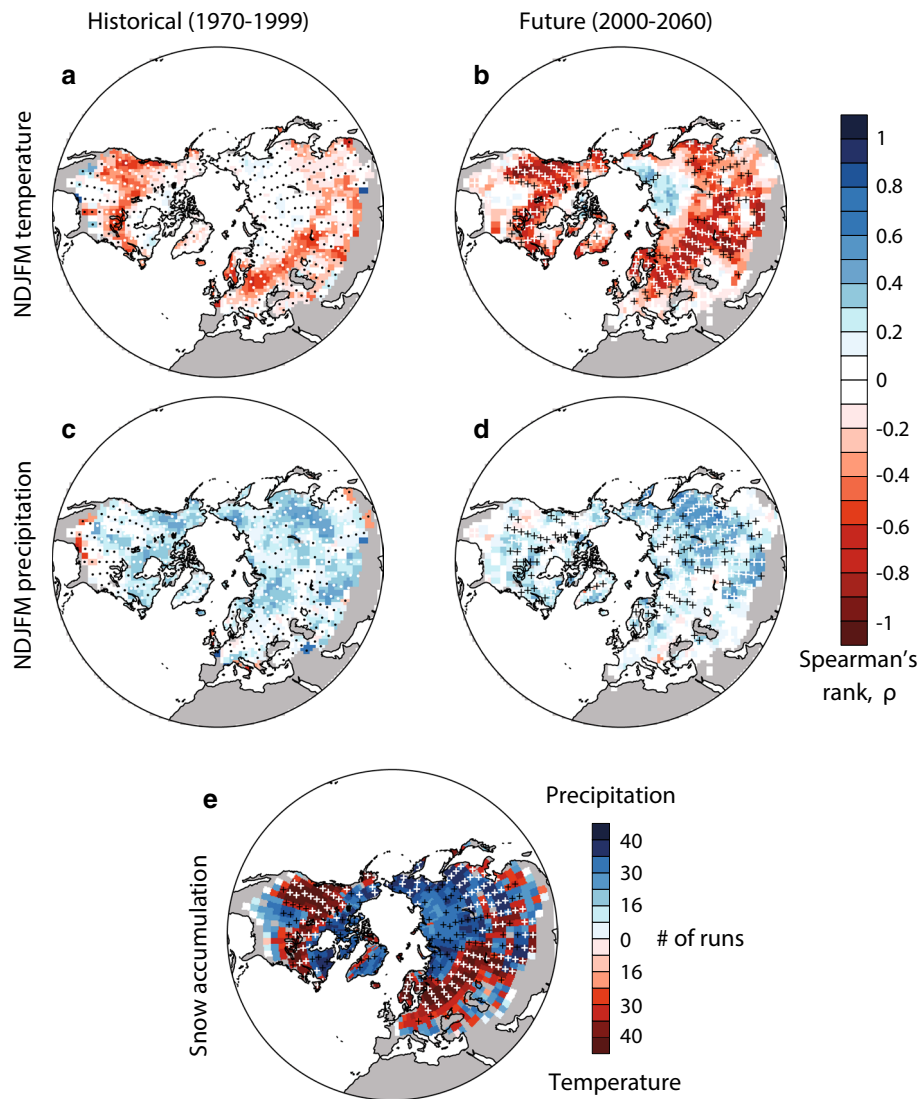


**Fig. 6** Partial correlations with accumulated snow. The Spearman's rank partial correlation coefficients for March net snow accumulation with seasonal (NDJFM) average temperature (a, b) and NDJFM precipitation (c, d) in the baseline and future integrations (left and right columns, respectively). For the baseline period (a, c), white (black) stippling indicates a statistically significant partial correlation at the 1 % (5 %) level. For the future period (b, d), stippling indicates the significance of the ensemble trends, with white (black) plus signs indicating an ensemble signal-to-noise of greater than two (one). Grey regions are areas where there is no net snow accumulation in the

baseline period. The number of integrations that show a higher snow accumulation correlation with temperature or with precipitation at a given grid point, 2000–2060 are shown in e. In e, at each grid point, we show the number of ensemble members that exhibit a stronger correlation with temperature (red) or with precipitation (blue) where more than half of the members with data at that grid point are more correlated with one than the other. Color shading indicates the number of realizations that show the correlation. The white (black) stippling indicates where more than half of the runs that do exhibit a stronger correlation are significant at the 1 % (5 %) level

mid-latitude grid points exhibit at least one realization with a statistically significant positive trend in March net snow accumulation, and at least one realization with a statistically significant negative trend in March net snow accumulation (Fig. 8a, b). Although the regional-scale ensemble mean response is robust (e.g., Figs. 3b, 4a), the range of possible outcomes in the individual realizations shows that natural variability creates uncertainty in the magnitude—and possibly direction—of sub-regional-scale snow trends

over the near-term decades, when adaptation is thought to have the greatest marginal benefits (Carter et al. 2007).

The trends in March net snow accumulation appear to be driven primarily by trends in cold-season temperature, which exhibit both less uncertainty than precipitation trends and greater agreement with the sign of the snow trends. Despite regional variability in the temperature response across the ensemble (Figs. 3a, 4a), nearly all ensemble members, grid points, and regions exhibit a

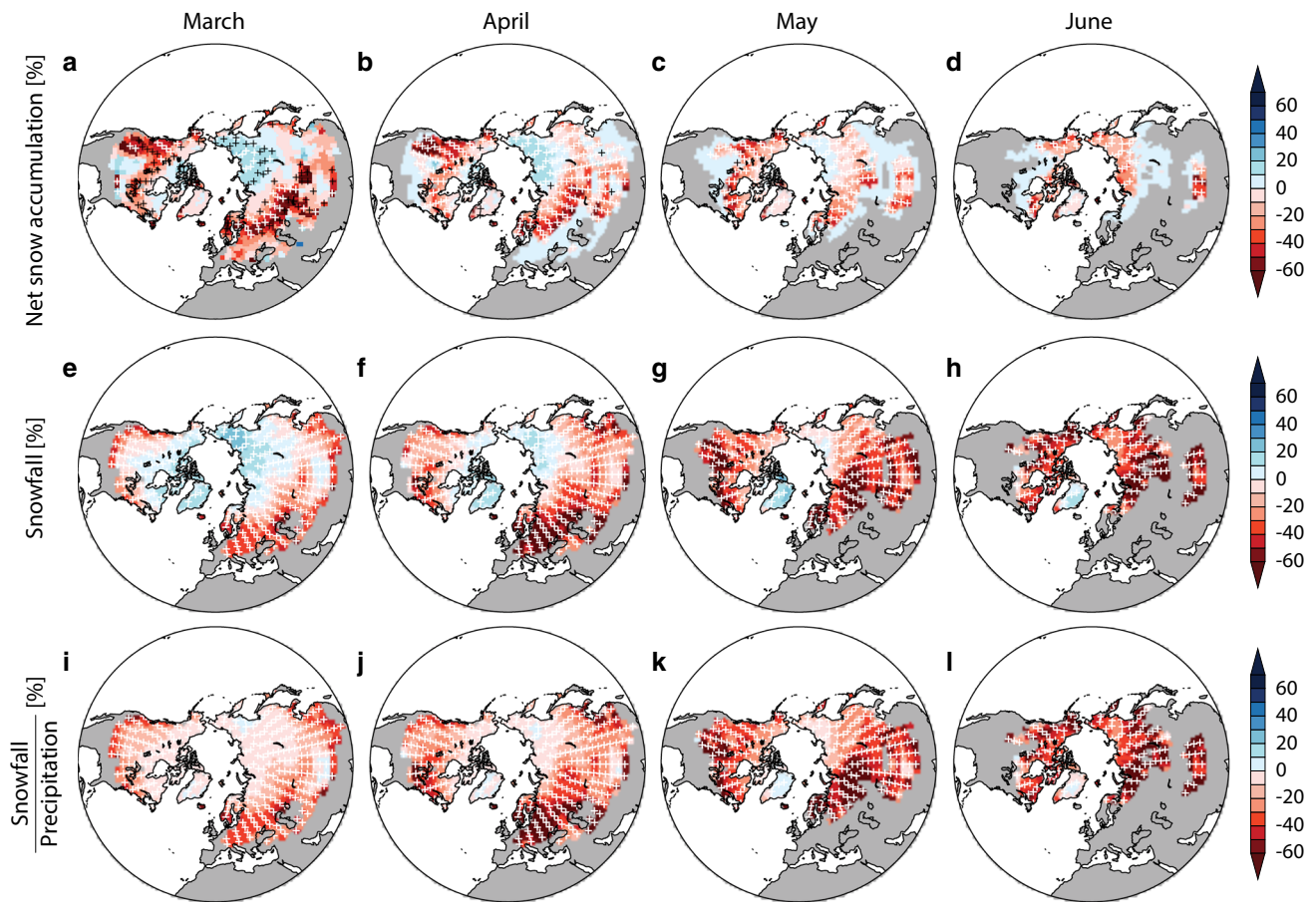


**Fig. 7** Late season net snow accumulation (**a–d**), snowfall (**e–h**), and snowfall-to-precipitation ratio (**i–l**) trends, as estimated in Fig. 5 (see “Methods”). Each plot shows the ensemble mean 50-year grid point linear trends for March (**a, e, i**), April (**b, f, j**), May (**c, g, k**), and June (**d, h, l**). The net snow accumulation values represent trends in the snow remaining on the ground in that month, summarizing cold-season snow accumulation and snowmelt in places with extended snow

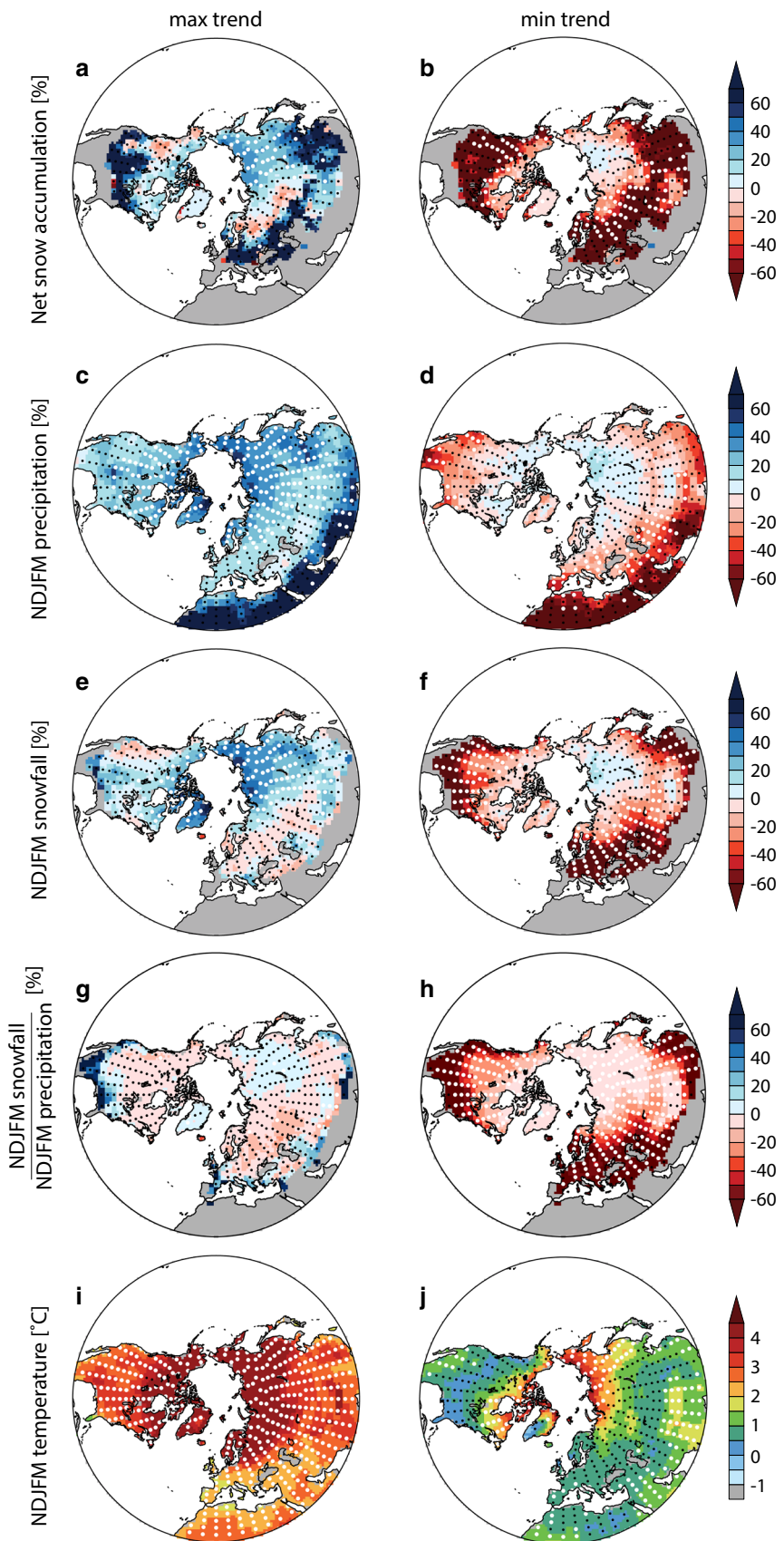
seasons. Snowfall and snowfall-to-precipitation ratio trends are fit to individual months, not cold-season (NDJFM) averages shown in other figures. Note that **a** is the same panel as in Fig. 5a. Grey indicates regions with no net snow accumulation in the baseline. Stippling indicates the significance of the ensemble-mean trend, with white (black) plus signs indicating an ensemble average trend greater than two (one) times the SD of all 40 individual trends

**Table 4** Uncertainty in multi-decadal regional changes induced by internal climate variability

Region	ΔNet snow (%)	ΔNDJFM temperature (°C)	ΔNDJFM precipitation (%)	ΔNDJFM snowfall (%)	ΔNDJFM ratio (%)
(1) Alaska	13.82	1.66	9.08	9.98	7.31
(2) Arctic Canada	7.54	1.11	8.75	4.95	3.04
(3) W. US	33.33	0.81	11.28	12.97	12.43
(4) E. US	18.34	0.80	10.50	12.19	7.99
(5) N. Europe	29.76	0.89	7.53	15.82	15.24
(6) N.E. Europe	12.94	1.32	7.17	5.53	8.00
(7) N.E. Asia	3.73	1.27	6.11	3.95	2.04
(8) Central Asia	30.76	0.73	14.17	22.85	19.18
(9) Greater Himalaya	15.98	0.56	7.39	7.47	3.66

Each value represents the run with the maximum change minus that with minimum change. Values are expressed as a percentage of the baseline mean

**Fig. 8** Grid point maximum and minimum linear trends. For March net snow accumulation (**a**, **b**), cold-season precipitation (**c**, **d**), snowfall (**e**, **f**), snowfall-to-precipitation ratio (**g**, **h**), and temperature (**i**, **j**), each grid point shows the value of the maximum (*left column*) and minimum (*right column*) linear 50-year trends from among the 40 ensemble members. *Each map*, therefore, is a composite of the 40-member ensemble. Stippling indicates the statistical significance of the linear trend at that grid point within the ensemble member from which it was pulled, with white (black) dots representing a trend significant at the 1 % (5 %) level



robust signal in cold-season surface temperature trends (Figs. 3a, 5c; Tables 2, 3). For example, according to Deser et al. (2012a), this large single-model ensemble can characterize mid-latitude winter temperature variability with as few as 3–6 ensemble members, far fewer than the minimum of 15 needed for precipitation. The robustness of the temperature response is evident at the sub-regional scale in our analyses, where the ensemble signal-to-noise in temperature trends is greater than 2 over all land areas (Fig. 5c).

Despite the robustness of the temperature trends, some areas do exhibit variations in the magnitude. For example, the intra-ensemble range of regional-scale trends is ~3 °C over Alaska and Northeastern Europe (Fig. 3a), suggesting that internal variability can damp or amplify the effects of global warming over large regions on multi-decadal time scales (Deser et al. 2012a). Likewise, many mid-latitude grid points exhibit statistically significant 50-year trends that range from less than 1.5 °C to greater than 2.5 °C across the ensemble (Fig. 8i, j), an ensemble spread that is driven by differing circulation anomalies arising from atmospheric noise (Deser et al. 2012b).

These increases in temperature could influence net snow accumulation both by decreasing the fraction of cold-season precipitation that falls as snow, and by increasing the rate of snowmelt during the cold season (Adam et al. 2009; Mote et al. 2005; Stewart 2009; Pierce and Cayan 2013; Diffenbaugh et al. 2012; Ashfaq et al. 2013; Rauscher et al. 2008). We find that the pattern and magnitude of cold-season snowfall trends are similar to those of net snow accumulation trends (Fig. 5a, d). The decreasing net snow accumulation can be explained at least in part by precipitation falling as rain rather than snow (Krasting et al. 2013; Kapnick and Delworth 2013). This transition is illustrated by the prevalence of decreasing cold-season snowfall in areas that exhibit decreasing net snow accumulation but increasing cold-season precipitation. Indeed, all 40 realizations exhibit mean declines in regional snowfall-to-precipitation ratios over all 9 regions, including the 2 regions that exhibit increases in snowfall (Arctic Canada and Northeastern Asia) (Figs. 3e, 4e). In addition, the ensemble spread from natural variability is generally smaller for cold-season snowfall-to-precipitation ratio than for net snow accumulation (Figs. 3, 4, 5, 8; Table 4), suggesting that the response of snowfall to global warming is more robust.

The large declines in snowfall-to-precipitation ratio are consistent with those found by the late twenty-first century in the CMIP5 RCP4.5 and RCP8.5 experiments (Krassing et al. 2013; Pierce and Cayan 2013). Further, the direction of change in snowfall-to-precipitation ratio is consistent at the regional scale (Table 3), and even at the sub-regional scale, where the trends are negative in all 40 realizations for the majority of grid points in the mid- and high-latitudes (Fig. 8g, h). Increases in cold-season precipitation

coupled with increases in the fraction falling as rain suggest increasing winter runoff, with implications for winter water storage (Barnett et al. 2005), spring and summer water availability (Diffenbaugh et al. 2012; Rauscher et al. 2008), and the potential for more frequent rain-on-snow events (Putkonen et al. 2009). However, our results suggest that internal variability can influence the magnitude of this response within a region (such as in Central Asia; Fig. 3c), where the trends in snowfall-to-precipitation ratio can vary by up to 50 % of the baseline value (Fig. 3e).

These robust trends in temperature and snow-to-precipitation ratio—rather than uncertainty from precipitation—are the dominating influence on regional net snow accumulation trends over the next half-century. Although hemispheric cold-season precipitation trends are positive in all realizations (Fig. 2c), internal variability creates uncertainty at smaller spatial scales (Figs. 3c, 5b). The uncertainty in these regional- and sub-regional-scale trends has been linked to persistent circulation anomalies (Deser et al. 2012b; Mudryk et al. 2013). In contrast, many high-latitude areas exhibit consistent increases in cold-season precipitation. Such increases have been linked to thermodynamic and dynamic responses and feedbacks from Arctic warming and sea ice loss (Serreze et al. 2000; Deser et al. 2010; Yin 2005; Held and Soden 2006).

The one region where near-term net snow trends appear to be clearly dominated by precipitation trends is Northeastern Eurasia. As in previous analyses (Deser et al. 2010; Brown and Mote 2009; Diffenbaugh et al. 2012; Räisänen 2007; Krassing et al. 2013), precipitation increases over the high-latitude areas of Northeastern Asia are associated with projected gains in March net snow accumulation, along with a greater number of grid points exhibiting larger snow-precipitation correlations than snow-temperature correlations (Fig. 6b, d). Even with robust cold-season warming, temperatures over this region remain sufficiently cold to support March snow accumulation, allowing the precipitation increases to lead to increases in net snow accumulation (Brown and Mote 2009; Deser et al. 2010; Diffenbaugh et al. 2012; Krassing et al. 2013).

However, the metric of March snow accumulation does not capture spatial variations in the length of the snow season, including with latitude, which may affect the trends in Northeastern Asia. Therefore, to test the sensitivity of our results to such variations, we analyze the late-season evolution of net snow accumulation, snowfall, and snowfall-to-precipitation ratio trends for the months of March, April, May, and June (Fig. 7). Like the March net snow accumulation variable we present elsewhere, the net snow accumulation calculations for these months (Fig. 7a–d) represent trends in the mean snow remaining on the ground in that month, summarizing cold-season snow accumulation and snowmelt in locations where the snow season extends

beyond March. The snowfall (Fig. 7e–h) and snowfall-to-precipitation ratio (Fig. 7i–l) values represent trends in their respective monthly mean values, not the trends in cold-season (NDJFM) averages presented elsewhere. Beginning in April, the Northeastern Asian interior shows a latitudinal contraction in snow accumulation trends (Fig. 7b–d) and snowfall (Fig. 7e–h), with 50-year June snow accumulation trends that are 20 % below the baseline. These results highlight that the signal associated with warming exerts a stronger influence on regional snow accumulation than the uncertainty from precipitation. Further, the pattern of increases in near-term spring snow accumulation coupled with late-season declines in high-latitude continental interiors (such as Northeastern Asia) could also be expected to occur in high-elevation mid-latitude regions. However, a major limitation is the ability of CCSM3 to accurately simulate the climate of those high-elevation regions given the model's coarse spatial resolution (see “[Caveats](#)”).

#### 4.2 Caveats

Given the influence of internal variability on the uncertainty of near-term snow trends, the results should be considered within the context of CCSM3's simulation of observed modes of climate variability. Researchers have extensively evaluated the model's ability to capture both the patterns and magnitudes of seasonal and inter-annual modes of variability in both the atmosphere and ocean (Collins et al. 2006; Deser et al. 2006). In general, CCSM3 reproduces a number of the major modes of observed variability, as well as the amplitude and patterns of the seasonal cycle (Collins et al. 2006). However, there are important patterns of seasonal and inter-annual variability that CCSM3 does not reproduce accurately, which may influence the model's snowfall production and/or snow accumulation. In particular, the periodicity of ENSO, whose negative phase (in conjunction with a negative NAO) can influence positive snow anomalies in the US and Europe (Seager et al. 2010), is more frequent in CCSM3 than in observations (Deser et al. 2006).

One approach to addressing the limitations of the global climate model resolution is to use the GCM-simulated fields as inputs to nested high-resolution climate and hydrology models (e.g., Akhtar et al. 2009; Ashfaq et al. 2010, 2013; Hayhoe et al. 2004; Rauscher et al. 2008). Such approaches appear to more accurately capture observed sub-regional heterogeneity of snow hydrology (Ashfaq et al. 2013), including snowfall, which is critical in regions with complex boundary conditions, such as Central Asia (Kapnick and Delworth 2013). Quantifying the influence of internal variability on near-term trends in snow accumulation requires a large number of realizations of a single model, which the CCSM3 experiment provides

for the full globe. Although multi-member high-resolution climate-hydrologic model simulations are becoming tractable, to date these have been limited to considerably smaller ensemble sizes and individual regions (e.g., Ashfaq et al. 2013). Given sufficient computational resources, a clear next step is to merge these two approaches by running large ensembles of high-resolution nested climate-hydrology experiments over multiple regions. Such experiments will provide insight into the extent to which large-scale atmosphere and ocean variability interact with fine-scale processes to shape the response of sub-regional-scale snow hydrology to near-term global warming.

## 5 Conclusions

We analyze a unique 40-member single-model ensemble climate model experiment to test the influence of internal climate system variability on the response of Northern Hemisphere snow accumulation to near-term global warming. Our analyses yield three key results about the irreducible uncertainty arising from internal climate system variability: First, uncertainty in the sign of regional precipitation change is insufficient to drive uncertainty in the sign of near-term regional-scale snow accumulation. Late-season snow accumulation decreases in all regions, including those that exhibit equivocal cold-season precipitation changes (the Western US, Central Asia, and the Greater Himalaya), or cold-season precipitation increases (Northeastern Asia). Second, the consistency in the regional snow accumulation response appears to be driven by robust regional-scale warming, which reduces the fraction of precipitation falling as snow. Third, despite regional-scale consistency in the sign of the snow accumulation response, internal variability can influence the magnitude of snow accumulation trends at the hemispheric and regional scales, and the magnitude and direction of snow accumulation trends at the sub-regional scale, including in areas where the mean response is highly robust across the ensemble.

Characterizing the irreducible uncertainty in near-term changes in snow conditions is critical for effectively allocating resources to manage evolving climate-related risks. Adapting to near-term snow changes will likely require regional and local responses that integrate both the long-term trend and the influence of internal climate system variability. Such responses potentially encompass institutional, social, and economic changes, as well as new hydrological infrastructure—all of which can require long time horizons to be implemented. Characterizing the probability of differing potential outcomes is one means to inform such adaptive response. Our results suggest that, in order to be effective, adaptation actions will need to integrate both the robustness of the snow response at the regional-scale and

the possibility that internal variability could dominate snow trends at the local-scale.

**Acknowledgments** We thank two anonymous reviewers for their insightful and constructive comments. The CCSM3 simulations—called the “twenty-first century CCSM3 Large Ensemble Project”—were produced by the NCAR Climate Variability and Climate Change Working Group and were analyzed using computing resources provided by the Center for Computational Earth and Environmental Sciences (CEES) at Stanford University. We thank NCAR and the Earth System Grid Federation ([earthsystemgrid.org](http://earthsystemgrid.org)) for access to the CCSM3 simulations. The GLDAS-2 data used in this study were acquired as part of the mission of NASA’s Earth Science Division and archived and distributed by the Goddard Earth Sciences (GES) Data and Information Services Center (DISC). We acknowledge Felix Schönbrodt for his R statistical routine “visually-weighted regression,” (available here: <http://www.nicebread.de/visually-weighted-watercolor-plots-new-variants-please-vote/>). Our work was supported by the Margaret Jonsson Family Fellowship and NSF award 0955283.

## References

- Adam JC, Hamlet AF, Lettenmaier DP (2009) Implications of global climate change for snowmelt hydrology in the twenty-first century. *Hydrol Process* 972:962–972. doi:[10.1002/hyp.7201/full](https://doi.org/10.1002/hyp.7201/full)
- Akhtar M, Ahmad N, Booij MJ (2009) Use of regional climate model simulations as input for hydrological models for the Hindukush-Karakorum-Himalaya region. *Hydrol Earth Syst Sci* 13(7):1075–1089
- Alexander MA et al (2010) The atmospheric response to projected terrestrial snow changes in the late twenty-first century. *J Clim* 23(23):6430–6437. doi:[10.1175/2010JCLI3899.1](https://doi.org/10.1175/2010JCLI3899.1)
- Ashfaq M et al (2010) Influence of climate model biases and daily-scale temperature and precipitation events on hydrological impacts assessment: a case study of the United States. *J Geophys Res* 115(D14):D14116. doi:[10.1029/2009JD012965](https://doi.org/10.1029/2009JD012965)
- Ashfaq M et al (2013) Near-term acceleration of hydroclimatic change in the western U.S. *J Geophys Res Atmos* 118:1–18. doi:[10.1002/jgrd.50816](https://doi.org/10.1002/jgrd.50816)
- Barnett TP, Adam JC, Lettenmaier DP (2005) Potential impacts of a warming climate on water availability in snow-dominated regions. *Nature* 438(7066):303–309
- Barnett TP et al (2008) Human-induced changes in the hydrology of the western United States. *Science* 319:1080–1083
- Bohr GS, Aguado E (2001) Use of April 1 SWE measurements as estimates of peak seasonal snowpack and total cold-season precipitation. *Water Resour Res* 37(1):51–60. doi:[10.1029/2000WR900256/full](https://doi.org/10.1029/2000WR900256/full)
- Bony S, Colman R, Kattsov V (2006) How well do we understand and evaluate climate change feedback processes? *J Clim* 19:3445–3482. doi:[10.1175/JCLI3819.1](https://doi.org/10.1175/JCLI3819.1)
- Brown RD, Mote PW (2009) The response of Northern Hemisphere snow cover to a changing climate. *J Clim* 22(8):2124–2145. doi:[10.1175/2008JCLI2665.1](https://doi.org/10.1175/2008JCLI2665.1)
- Cane MA (2010) Climate science: decadal predictions in demand. *Nat Geosci* 3(4):231–232
- Carter TR (2007) et al New assessment methods and the characterisation of future conditions. In: Parry ML et al. (eds) Climate change 2007: impacts, adaptation and vulnerability. Contribution of working group II to the fourth assessment report of the intergovernmental panel on climate change. Cambridge University Press, Cambridge, pp 133–171
- Cohen JL et al (2012) Arctic warming, increasing snow cover and widespread boreal winter cooling. *Environ Res Lett* 7(1):014007
- Collins WD et al (2004) Description of the NCAR community atmosphere model (CAM 3.0). [http://hanson.geog.udel.edu/~hanson/hanson/CLD\\_GCM\\_Experiment\\_S11\\_files/description.pdf](http://hanson.geog.udel.edu/~hanson/hanson/CLD_GCM_Experiment_S11_files/description.pdf). Accessed 5 Nov 2013
- Collins WD et al (2006) The community climate system model version 3 (CCSM3). *J Clim* 19:2122–2143. doi:[10.1175/JCLI3761.1](https://doi.org/10.1175/JCLI3761.1)
- Deser C et al (2006) Tropical Pacific and Atlantic climate variability in CCSM3. *J Clim* 19:2451–2481. doi:[10.1175/JCLI3759.1](https://doi.org/10.1175/JCLI3759.1)
- Deser C et al (2010) The seasonal atmospheric response to projected Arctic sea ice loss in the late twenty-first century. *J Clim* 23(2):333–351. doi:[10.1175/2009JCLI3053.1](https://doi.org/10.1175/2009JCLI3053.1)
- Deser C et al (2012a) Uncertainty in climate change projections: the role of internal variability. *Clim Dyn* 38(3–4):527–546. doi:[10.1007/s00382-010-0977-x](https://doi.org/10.1007/s00382-010-0977-x)
- Deser C et al (2012b) Communication of the role of natural variability in future North American climate. *Nat Clim Change* 2:775–780
- Diffenbaugh NS, Field CB (2013) Changes in ecologically critical terrestrial climate conditions. *Science* 341:486–492
- Diffenbaugh NS et al (2005) Fine-scale processes regulate the response of extreme events to global climate change. *Proc Natl Acad Sci USA* 102(44):15774–15778
- Diffenbaugh NS, Scherer M, Ashfaq M (2012) Response of snow-dependent hydrologic extremes to continued global warming. *Nat Clim Change* 3(11):379–384
- Fletcher CG et al (2009) Circulation responses to snow albedo feedback in climate change. *Geophys Res Lett* 36(9):L09702. doi:[10.1029/2009GL038011](https://doi.org/10.1029/2009GL038011)
- Füssel H-M (2007) Adaptation planning for climate change: concepts, assessment approaches, and key lessons. *Sustain Sci* 2(2):265–275. doi:[10.1007/s11625-007-0032-y](https://doi.org/10.1007/s11625-007-0032-y)
- Hall A, Qu X (2006) Using the current seasonal cycle to constrain snow albedo feedback in future climate change. *Geophys Res Lett* 33(3):L03502
- Hall A, Qu X, Neelin JD (2008) Improving predictions of summer climate change in the United States. *Geophys Res Lett* 35(1):L01702
- Hamlet AF et al (2005) Effects of temperature and precipitation variability on snowpack trends in the Western United States. *J Clim* 18(21):4545–4561. doi:[10.1175/JCLI3538.1](https://doi.org/10.1175/JCLI3538.1)
- Hartmann DL, Tank AMGK, Rusticucci M (2013) Chapter 2: observations: atmosphere and surface. In: Working group I contribution to the IPCC 5th assessment report “climate change 2013: the physical science basis”, p 165
- Hatfield JL et al (2011) Climate Impacts on agriculture: implications for crop production. *Agron J* 103(2):351–370
- Hawkins E, Sutton R (2009) The potential to narrow uncertainty in regional climate predictions. *Bull Am Meteorol Soc* 90(8):1095–1107. doi:[10.1175/2009BAMS2607.1](https://doi.org/10.1175/2009BAMS2607.1)
- Hawkins E, Sutton R (2010) The potential to narrow uncertainty in projections of regional precipitation change. *Clim Dyn* 37(1–2):407–418. doi:[10.1007/s00382-010-0810-6](https://doi.org/10.1007/s00382-010-0810-6)
- Hayhoe K et al (2004) Emissions pathways, climate change, and impacts on California. *Proc Natl Acad Sci USA* 101(34):12422–12427
- Held IM, Soden BJ (2006) Robust responses of the hydrological cycle to global warming. *J Clim* 19:5686–5699
- Howat IM, Tulaczyk S (2005) Trends in spring snowpack over a half-century of climate warming in California, USA. *Ann Glaciol* 40(1):151–156
- Hsiang SM (2013) Visually-weighted regression. [http://papers.ssrn.com/sol3/papers.cfm?abstract\\_id=2265501](http://papers.ssrn.com/sol3/papers.cfm?abstract_id=2265501). Accessed 24 Jan 2014
- John VO, Soden BJ (2007) Temperature and humidity biases in global climate models and their impact on climate feedbacks. *Geophys Res Lett* 34(18):L18704. doi:[10.1029/2007GL030429](https://doi.org/10.1029/2007GL030429)
- Kapnick SB, Delworth TL (2013) Controls of global snow under a changed climate. *J Clim* 26(15):5537–5562. doi:[10.1175/JCLI-D-12-00528.1](https://doi.org/10.1175/JCLI-D-12-00528.1)

- Kapnick SB, Hall A (2011) Causes of recent changes in western North American snowpack. *Clim Dyn* 38(9–10):1885–1899. doi:[10.1007/s00382-011-1089-y](https://doi.org/10.1007/s00382-011-1089-y)
- Knutti R, Sedláček J (2012) Robustness and uncertainties in the new CMIP5 climate model projections. *Nat Clim Change* 3(4):369–373. doi:[10.1038/nclimate1716](https://doi.org/10.1038/nclimate1716)
- Krasting JP et al (2013) Future changes in Northern Hemisphere snowfall. *J Clim* 130520135404007. doi:[10.1175/JCLI-D-12-00832.1](https://doi.org/10.1175/JCLI-D-12-00832.1)
- Kunreuther H et al (2013) Risk management and climate change. *Nat Clim Change* 3(5):447–450. doi:[10.1038/nclimate1740](https://doi.org/10.1038/nclimate1740)
- Lawrence DM, Slater AG (2009) The contribution of snow condition trends to future ground climate. *Clim Dyn* 34(7–8):969–981. doi:[10.1007/s00382-009-0537-4](https://doi.org/10.1007/s00382-009-0537-4)
- Meehl GA et al (2006) Climate change projections for the twenty-first century and climate change commitment in the CCSM3. *J Clim* 19(11):2597–2616. doi:[10.1175/JCLI3746.1](https://doi.org/10.1175/JCLI3746.1)
- Meehl GA et al (2009) Decadal prediction. *Bull Am Meteorol Soc* 90(10):1467–1485. doi:[10.1175/2009BAMS2778.1](https://doi.org/10.1175/2009BAMS2778.1)
- Mote PW (2006) Climate-driven variability and trends in mountain snowpack in Western North America. *J Clim* 19:6209–6220
- Mote PW et al (2005) Declining mountain snowpack in Western North America. *Bull Am Meteorol Soc* 86(1):39–49. doi:[10.1175/BAMS-86-1-39](https://doi.org/10.1175/BAMS-86-1-39)
- Mudryk LR, Kushner PJ, Derksen C (2013) Interpreting observed northern hemisphere snow trends with large ensembles of climate simulations. *Clim Dyn*. doi:[10.1007/s00382-013-1954-y](https://doi.org/10.1007/s00382-013-1954-y)
- Oleson KW et al (2004) Technical description of the Community Land Model (CLM). NCAR Technical Note NCAR/TN-461+STR. National Center for Atmospheric Research, Boulder, CO
- Peters GP et al (2013) The challenge to keep global warming below 2°C. *Nat Clim Change* 3(1):4–6. doi:[10.1038/nclimate1783](https://doi.org/10.1038/nclimate1783)
- Pierce DW, Cayan DR (2013) The uneven response of different snow measures to human-induced climate warming. *J Clim* 26(12):4148–4167. doi:[10.1175/JCLI-D-12-00534.1](https://doi.org/10.1175/JCLI-D-12-00534.1)
- Putkonen J et al (2009) Rain on snow: little understood killer in the north. *Eos* 90(26):221–228
- Qu X, Hall A (2007) What controls the strength of snow-albedo feedback? *J Clim* 20(15):3971–3981. doi:[10.1175/JCLI4186.1](https://doi.org/10.1175/JCLI4186.1)
- Räisänen J (2007) Warmer climate: less or more snow? *Clim Dyn* 30(2–3):307–319. doi:[10.1007/s00382-007-0289-y](https://doi.org/10.1007/s00382-007-0289-y)
- Rauscher SA et al (2008) Future changes in snowmelt-driven runoff timing over the western US. *Geophys Res Lett* 35(16):L16703. doi:[10.1029/2008GL034424](https://doi.org/10.1029/2008GL034424)
- Rodell M, Houser P (2004) The global land data assimilation system. *Bull Am Meteorol Soc* 381–394. doi:[10.1175/BAMS-85-3-381](https://doi.org/10.1175/BAMS-85-3-381)
- Roesch A (2006) Evaluation of surface albedo and snow cover in AR4 coupled climate models. *J Geophys Res* 111:D15111. doi:[10.1029/2005JD006473](https://doi.org/10.1029/2005JD006473)
- Rogelj J, Meinshausen M, Knutti R (2012) Global warming under old and new scenarios using IPCC climate sensitivity range estimates. *Nat Clim Change* 2(4):248–253. doi:[10.1038/nclimate1385](https://doi.org/10.1038/nclimate1385)
- Rood SB et al (2008) Declining summer flows of Rocky Mountain rivers: changing seasonal hydrology and probable impacts on floodplain forests. *J Hydrol* 349(3–4):397–410
- Rupp DE et al (2013) Detection and attribution of observed changes in Northern Hemisphere spring snow cover. *J Clim* 26:6904–6914. doi:[10.1175/JCLI-D-12-00563.1](https://doi.org/10.1175/JCLI-D-12-00563.1)
- Santer BD et al (2000) Statistical significance of trends and trend differences in layer-average atmospheric temperature time series. *J Geophys Res* 105(D6):7337. doi:[10.1029/1999JD901105](https://doi.org/10.1029/1999JD901105)
- Scherrer SC, Appenzeller C (2006) Swiss Alpine snow pack variability: major patterns and links to local climate and large-scale flow. *Clim Res* 32:187–199
- Seager R et al (2010) Northern Hemisphere winter snow anomalies: ENSO, NAO and the winter of 2009/10. *Geophys Res Lett* 37(14):n/a–n/a. doi:[10.1029/2010GL043830](https://doi.org/10.1029/2010GL043830)
- Serreze M, Walsh J, Chapin FS (2000) Observational evidence of recent change in the northern high-latitude environment. *Clim Change* 46:159–207. doi:[10.1023/A:1005504031923](https://doi.org/10.1023/A:1005504031923)
- Sheffield J et al (2004) A simulated soil moisture based drought analysis for the United States. *J Geophys Res* 109(D24):D24108. doi:[10.1029/2004JD005182](https://doi.org/10.1029/2004JD005182)
- Siegfried T et al (2011) Will climate change exacerbate water stress in Central Asia? *Clim Change* 112(3–4):881–899. doi:[10.1007/s10584-011-0253-z](https://doi.org/10.1007/s10584-011-0253-z)
- Sobolowski S, Gong G, Ting M (2010) Modeled climate state and dynamic responses to anomalous North American snow cover. *J Clim* 23(3):785–799. doi:[10.1175/2009JCLI3219.1](https://doi.org/10.1175/2009JCLI3219.1)
- Stewart IT (2009) Changes in snowpack and snowmelt runoff for key mountain regions. *Hydrol Process* 94:78–94. doi:[10.1002/hyp.7128/full](https://doi.org/10.1002/hyp.7128/full)
- Tague C, Peng H (2013) The sensitivity of forest water use to the timing of precipitation and snowmelt recharge in the California Sierra: implications for a warming climate. *J Geophys Res Biogeosci* 118(2):875–887. doi:[10.1002/jgrb.20073](https://doi.org/10.1002/jgrb.20073)
- Taylor RG (2013) Ground water and climate change. *Nat Clim Change* 3:322–329
- Viviroli D et al (2007) Mountains of the world, water towers for humanity: typology, mapping, and global significance. *Water Resour Res* 43:W07447. doi:[10.1029/2006WR005653](https://doi.org/10.1029/2006WR005653)
- Westerling AL et al (2006) Warming and earlier spring increase western U.S. forest wildfire activity. *Science* 313(5789):940–943
- Yin JH (2005) A consistent poleward shift of the storm tracks in simulations of 21st century climate. *Geophys Res Lett* 32(18):L18701. doi:[10.1029/2005GL023684](https://doi.org/10.1029/2005GL023684)